Development of a Prognostic Model Based on Differentially Expressed Immune Genes of Lung Adenocarcinoma

Yang Zhai
Tumor Hospital of Shaanxi Province
Lina Li
Tumor Hospital of Shaanxi Province
Yuzhen Wang
Tumor Hospital of Shaanxi Province
Jingjin Li
Xi'an Jiaotong University Medical College
Xu Li
Tumor Hospital of Shaanxi Province
Bin Liu
Xi'an Jiaotong University
Yili Zhang
Tumor Hospital of Shaanxi Province
Qian Chen (chenqian1006@126.com)
Xi'an Jiaotong University Medical college

Research Article

Keywords: lung adenocarcinoma, prognosis, DEIG, TCGA, immune infiltration

Posted Date: October 18th, 2021

DOI: https://doi.org/10.21203/rs.3.rs-966516/v1

Abstract

Due to the enormous heterogeneity and molecular complexity, the efficacy of existing lung adenocarcinoma risk prediction models were less than satisfactory.

In this study, we downloaded the immune-related genes were from InnateDB, and the differentially expressed immune genes (DEIGs) were analyzed with edgeR and DESeq2 algorithm. In total, 1359 DEIGs were identified. Cytoscape was employed to build a mRNA-miRNA-lncRNA network which was consists of 8 lncRNAs, 7 miRNAs and 117 DEIGs. Functional enrichment analysis indicated that the 117 DEIGs were involved in immune and inflammatory responses and actively involved in a *MAPK* signaling pathway. A prognostic signature based on ten DEIGs including *ASPH*, *CAV1*, *FKBP4*, *GRIK2*, *FURIN*, *SLC6A8*, *FSCN1*, *CKAP4*, *HAPLN2* and *IL22RA2* which performed well was correlated with tumor burden, tumor stage and metastasis. The similar result was obtained in the validation dataset GSE72094 ($p<0.0001$). The prognostic index reflected infiltration by B cell, CD4+T cell, CD8+T cell and dendritic cell. We also found that *ASPH* and *FSCN1* were over-expression in A549, H1299, PC-9 cells, and the positive expression of *ASPH*, *FSCN1*, *MS4A1* and *CD40LG* had a correlation with the TNM stage, cellular differentiation and the lymphnode metastasis($p<0.05$). High levels of *ASPH* and *FSCN1*, low levels of *MS4A1* and *CD40LG* expression are all associated with poor overall survival in LUAD ($p<0.05$).

In conclusion, our results identified DEIGs of clinical significance, verified the effect of the DEIGs-based, personalized prediction model for lung adenocarcinoma prognosis. Together, our results revealed that ASPH and FSCN1 could be a prognostic marker for lung adenocarcinoma.

Introduction

Lung cancer is the most common cause of cancer deaths globally. There were 2.2 million incident cases of lung cancer and 1.9 million deaths in 2017. From 2007 to 2017, lung cancer cases increased by 37% (1, 2), in which adenocarcinoma accounts for 40% of all cases, and its incidence rate is on the rise (3). Nearly 33%-52% of patients die within five years even with complete surgical resection (4). It remains a huge burden on the healthcare system and a significant unmet medical need. In recent years, tumor immunotherapy has become a very important therapeutic strategy for many types of cancer (5–7). Based on a number of clinical studies, immunotherapy, such as blockade of immune checkpoint therapy, has been approved by FDA for using in lung cancer recently (8–10). However, only a small patient population can benefit from immunotherapy, limiting its clinical application. Therefore, it is important to find biomarkers that can reliably predict the prognosis and patient survival.

Extensive research show that immune microenvironment and immunogenomics play a key role in the development of tumor (11), the prognostic impact of the immune microenvironment in lung cancer has also been demonstrated (12). While these results analysed the significance of immunology in lung adenocarcinoma, the molecular mechanisms still remain unclear, particularly with regards to immunogenomic effects. Although previous studies have reported survival stratification based on the immune-related gene expression in patients with lung adenocarcinoma (13, 14), deeper verification is still lacking.

In this study, we combined multiple datasets from TCGA to develop and validate an individualized prognostic signature for LUAD. We systematically analyzed the expression and prognostic value of DEIGs and built an effective prognostic index for LUAD. Our aim is to delve deep into the clinical application value of DEIGs and their potential as biomarkers on prognostic stratification. Our results could improve the estimation of lung adenocarcinoma prognosis and offer a foundation for further immune-related research.

Materials And Methods

All methods were carried out in accordance with relevant guidelines and regulations. The studies involving human participants were reviewed and approved by Ethics Committee of Tumor Hospital of Shaanxi Province. Written informed consent for participation was waived for this study by Ethics Committee of Tumor Hospital of Shaanxi Province in accordance with the national legislation and the institutional requirements.

Data preprocessing

The RNA-Seq, miRNA-Seq, somatic mutation datasets as well as the clinical information for LUAD patients were downloaded from NCI's Genomic Data Commons (GDC) (https://portal.gdc.cancer.gov) using R package 'TCGA biolinks' (15), and only "Primary solid Tumor" and "Solid Tissue Normal" samples were included. LncRNAs were extracted from the gene expression profiles with lncRNAs annotations downloaded from gencode (16) (https://www.gencodegenes.org). Furthermore, a total of 7477 immune-related genes were derived from InnateDB (17)(https://www.innatedb.com). While the estimated infiltration abundance of immune cells of LUAD samples were obtained by TIMER (18)(https://cistrome.shinyapps.io/timer/).

Identification of Differentially expressed RNAs and enrichment of gene sets

Differentially expressed RNAs were detected using DESeq2 (19) and edgeR (20). RNAs with '|log2(fold change)| > 1', 'p value < 0.05' and 'fdr < 0.3' in both methods were considered to be differentially expressed. The R package 'ClusterProfiler' (21) was employed for pathway enrichment analysis with differentially expressed genes.

Annotation of RNA interactions

The lncRNA/microRNA interaction was predicted with starBase v3.0 (22). The R package miRNAtap was utilized to predict the targeted mRNAs of microRNAs. Five databases were included in the analysis, including PicTar, DIANA, TargetScan, miRanda and miRDB. Outputs were miRNA/mRNA interactions reported consistently in at least three out of five databases. KEGG database was used for pathway enrichmen(23). GO Biological Pathway (BP) enrichment was performed to unravel the biological pathways.

ceRNA network construction

The lncRNA-miRNA-mRNA network was constructed with the differentially expressed lncRNAs, their potential targeted miRNAs, and the targeted mRNAs of miRNAs as well. The interactions between DElncRNA and DEmiRNA were predicted by starBase v3.0. Target genes of DEmiRNA were predicated by miRNAtap. Cytoscape (v3.7.2) (24) was employed for the network visualization. More specifically, a table of RNA interactions including the source and target RNAs, as well as the log2(fold change) in different groups was created as the input. Once imported into the software, the source and target RNAs were used to construct the interaction network, with color and shapes of nodes indicating different attributes of the RNA.

PPI network construction and hub-genes identification

The PPI network was built with genes in the ceRNA network with STRING (v11.0) (25). Afterwards, the edge file was downloaded and imported into Cytoscape. And hub-genes were clustered by MCODE App in Cytoscape, with 3 as the “Degree cutoff”.

Construction of immune signatures

We used the 117 differentially expressed mRNA preserved in the final ceRNA network as input for model construction. The total TCGA LUAD patient cohort was randomly sampled to obtain 70% patients of training set and 30% patients of test set. The GSE72094 queue serves as the validation data set. Then the prediction model was built on the most frequent gene set with effective coefficients in the lasso regression using R package ‘glmnet’ (26) for 1000 iterations on the training dataset. The function “cv.glmnet” was employed to perform 10-fold cross-validation of glmnet. The risk score was defined as the sum of the normalized expression of genes multiplied by their coefficients in the gene set. Receiver operating characteristic curve (ROC) was used to evaluate the cutoff of risk scores as a predicting factor for the survival of LUAD patients at five years prior to death. After dividing the patient into two groups according to the risk score, ‘Survminer’ was employed for survival analysis for both training and testing data. Statistical analysis was performed by R (3.6.1). Heatmaps were generated using R package pheatmap (1.0.12).

Univariate and Multivariate cox regression

Cox proportional hazards modeling was applied to investigate the relationship between predictor variables and survival time. The correlations among predictor variables were adjusted in multivariate cox regression. The categorical variables were transformed into numeric ones before cox regression. For example, Stage I converted to “1”, Stage II converted to “2”, Stage III converted to “3”, and Stage IV converted to “4”. The Staging variable was then treated as a numeric variable in the regression analysis.

Cell culture

The Human Bronchial Epithelioid Cells, BEAS-2B and human NSCLC cell lines, H1299, PC9, A549, were purchased from the American Type Culture Collection (ATCC; Manassas, VA, USA). The cells were cultured in RPMI- 1640 or DMEM medium (Hyclone, UT, USA) supplemented with 10% fetal bovine serum (FBS; Transgenomic Co., Shanghai, China) at 37°C in a humidified incubator containing 5% CO2 in air. Cells were replenished daily with fresh medium and were harvested by trypsinization and split at a 1:3 ratio with fresh medium every 2 d (27, 28).

Western blot analysis

After drug treatment, cells were harvested in ice-cold PBS and lysed with radioimmunoprecipitation assay buffer con- taining protease and phosphatase inhibitors, then centrifuged (12,000 rpm, 20 minutes) at 4°C. The protein supernatant was collected and its concentration determined using BCA protein assay reagent (both from Wolsen Company, Xi’an, People’s Republic of China). Each protein sample was subjected to sodium dodecyl sulfate polyacrylamide gel electrophoresis (8–12%), then transferred onto polyvinylidene difluoride membranes (EMD Millipore, Billerica, MA, USA), blocked with 10% non-fat milk in 0.05% Tris-based saline-Tween 20 for 2 hours at RT. Membranes were labeled with primary antibodies against *ASPH*, *FSCN1* (1:1000, Santa Cruz Biotechnology), and anti-GAPDH (1:1000, Santa Cruz Biotechnology) overnight at 4°C (29). Subsequently, blots were washed with Tris-based saline-Tween 20 for 30–40 minutes, then further probed with secondary antibody at RT for 1 hour and subjected to reaction with enhanced chemiluminescence solution and visualized using ChemiDoc XRS+ system (BioRad Laboratories Inc., Hercules, CA, USA). For quantification of specific protein bands, films were scanned and analyzed using Labworks software (Mission Viejo, CA, USA) (30, 31).

Reverse transcription-quantitative polymerase chain reac- tion (RT-qPCR).

The total RNA (1,248.52 ng/μl) from cells was extracted using RNA Fast200 (Sigma-Aldrich; Merck Millipore). The PCR amplification reaction mixture (10 μl) contained the following: 5*PrimeScript buffer (2 μl), Prime- Script RT enzyme mix (0.5 μl), oligo dT primer (0.5 μl), random hexanucleotide (0.5 μl), total RNA (4 μl) and RNase Free (Takara Bio, Inc., Otsu Japan). The thermal cycler conditions were as follows: 94°C for 2 min then 35 cycles alternating between 94°C for 30 sec, 60°C for 30 sec, 72°C for 30 sec and 72°C for 2 min. The target gene expression levels were normalized to GAPDH levels. The formula 2ss(-ΔCq)=2[Cq (GAPDH)-Cq(target)] was used to calculate the relative gene expression levels for each sample, reflecting the normalized target gene expression levels (32,33). The primer sequences of ASPH were as follows: Upstream, 5'- CATGGAGGACACAAGAATGGG-3'; downstream, 5'- CCAAACGACAGCTACAGATGT-3'. The primer sequences of FSCN1 were as follows: Upstream, 5'- CTGCTACTTTGACATCGAGTGG-3'; downstream, 5'- GGGCGGTTGATGAGCTTCA-3'.

Immunohistochemistry

A total of 60 patients of LUAD getting surgery with no prior chemotherapy or radiotherapy at Tumor Hospital of Shaanxi Province were recruited in the study between January 2014 and December 2015. A mouse polyclonal anti-ASPH and anti-CD40LG antibody at a dilution of 1:50, anti-FSCN1 and anti-MS4A1 antibody at a dilution of 1:100 (all from Santa Cruz Biotechnology, INC), which were specific for immunohistochemistry. PBS was used to displace the primary antibody as the negative control. The Histological diagnosis was performed by 3 independent, experienced pathologists for all the cases. The Immunohistochemistry (IHC) technique was performed as previously described (34). 5 μm-thick sections were cut from the human lung adenocarcinoma

tissue and fixed in 10% buffered formalin overnight and paraffin-embedded. The slides were deparaffinized and rehydrated in graded alcohols, followed by antigen retrieval in a microwave oven. Slides were blocked with 10% normal goat serum for 20 minutes at 37°C to reduce nonspecific binding. The slides were incubated overnight at 4°C (35). After being washed, Horseradish peroxidase (HRP) conjugated goat anti-rabbit IgG was used as secondary antibody, and then visualized with 3,3'-diaminobenzidine (DAB) solution. Finally, hematoxylin was used to counterstain the section. The percentage of positive cells was classified into 5 score ranges: <10% (0),10–25% (1), 25–50% (2), 50–75% (3), and >75% (4). The intensity of staining was divided into 4 groups: no staining (0), light brown (1), brown (2), and dark brown (3). The staining positivity was determined using immunoreactivity score (IRS) which is the product of intensity score and quantity score. An overall score of >6 as strong positive, >3 as weak positive, and ≤3 was defined as negative.

Results

Identification of differentially expressed DEIGs

TCGA LUAD dataset legacy-archive (hg19) was downloaded, including four datasets: RNA count, miRNA count, somatic mutation and somatic CNV (Table S1). Gene expression data of “Primary solid Tumor” and “Solid Tissue Normal” samples were accessed by R package “TCGA biolinks”.The DEIGs were identified by obtaining the overlapping subset of a list of immune-related genes from InnateDB and the list of different expressed genes. A total of 7477 immune-related genes were downloaded from InnateDB. The differentially expressed gene analysis was performed by edgeR and DESeq2, and only DEIGs detected by both methods were included. A total of 1359 differentially expressed genes were identified, 713 up-regulated and 646 down-regulated (Table 1). As expected, functional enrichment analysis indicated that the cytokine-cytokine receptor interactions and the inflammatory pathways were among the top terms enriched by DEIGs. (Figure1)

Table 1
A total of 1359 differentially expressed genes were identified, 713 up-regulated and 646 down-regulated

	DEmRNA		DElncRNA		DEmiRNA
	Immune	Others	Immune	Others	
Tumor-up	713	1723	3	18	163
Tumor-down	646	1095	1	6	55

Construction of mRNA-miRNA-lncRNA Network

Cytoscape was employed to build a mRNA-miRNA-lncRNA network using differentially expressed lncRNA, miRNA and immune-related target mRNA (Figure 2). In total, the ceRNA network consisted of 8 lncRNA (*AGAP11*, *CASC2*, *GAS5, MIAT*, *PVT1*, *SNHG1*, *SNHG12*, *SNHG3*),7 miRNA(*hsa-mir-1276, hsa-mir-133b, hsa-mir-137, hsa-mir-451a, hsa-mir-543, hsa-mir-551a, hsa-mir-577*) and 117 target mRNA. (Table 2)

Table 2
The network was conducted by DElncRNA, DEmiRNA and immune-related DEmRNA with cytoscape

RNAtype	lncRNA	miRNA	mRNA
No.	8	7	117

Characteristics of target genes

As expected, the DEIGs were mainly involved in immune and inflammatory responses by using gene functional enrichment analysis. The most frequent biological terms among biological processes, cellular components, and molecular functions were “myeloid cell differentiation,” “cytoplasmic region” and “protein heterodimerization activity”(Figure 3A). For KEGG enrichment, MAPK signaling pathway was the most often enriched by differentially expressed target genes (Figure 3B). The 117 target genes were used to construct a protein-protein interaction network. Two subnetworks were extracted via MCODE algorithms. The first MCODE network had six proteins, *SH3GL2*, *TFRC*, *SYT1*, *FZD4* and *REPS2*. The second MCODE network had five components, *PDIA6*, *CDH2*, *CKAP4*, *CP* and *SPP1*(Figure S1). The mutations of those 117 target genes were investigated in 569 tumors. The top 50 genes were visualized using OncoPrint. Different mutation type was indicated by different color, and the missense mutation is the most common type (Figure S2).

Evaluation of clinical outcomes

The optimized model consisted of the following genes: *ASPH*, *CAV1*, *FKBP4*, *GRIK2*, *FURIN*, *SLC6A8*, *FSCN1*, *CKAP4*, *HAPLN2*, *IL22RA2*, which could serve as prognostic marker for LUAD patients. The area under curve of the receiver operating characteristic (ROC) curve was 0.699 for 3years, 0.627 for 5 years, 0.681 for 10years, indicating the prognostic model based on DEIGs has definite potential in survival monitoring. The heatmaps showed that the gene expression profiles were different between the cases of the high and low risk score groups (Figure 4). Univariate Cox regression analysis suggested that the prognostic

signature, age, tumor stage, pathologic stage and metastasis status are all associated with prognosis(Table 3).The prognostic model based on DEIGs was identified as an independent predictor using multivariate cox regression analysis after the adjustment of other parameters(Figure 5). We validated our model and selected genes using two additional datasets from GEO database. We obtained significant results in GSE72094(Figure S3).

Table 3
Univariate cox regression analysis

	HR	95%CI	p.value
RiskScore	12	(6.4-24)	7.9e-14
TMB	0.97	(0.9-1)	0.46
T	1.5	(1.3-1.8)	7.8e-06
M	2.2	(1.3-3.7)	0.0047
N	1.7	(1.4-2)	1.9e-09
Age	1	(0.99-1)	0.48
Stage	1.7	(1.5-1.9)	4.9e-13
Smoke	0.92	(0.67-1.3)	0.59
Gender	1.1	(0.79-1.4)	0.68

Correlation between Prognostic Signature and Immune Infiltration

We analyzed the relationship between model predicted risk score and immune cell infiltration to verify the function of immune related genes in tumor immune microenvironment. As shown in the figure 6, to some extent, the risk score of our model is inversely related to the infiltration of the immune cells including B cell (R= -0.32, p=2.1e-13), CD4+ T cell (R= -0.15, p=0.00067) and dendritic cell (R= -0.11, p=0.014) (Figure 6). The higher the risk score, the lower the amount of these immunoinfiltrating cells. The correlation was more significant in B cells as well as the cell markers, the markers such as *CD1D*, *CD5*, *CD19*, *MS4A1*, *CD27*, *CD40LG*, *CR2* were all negatively correlated with the model predicted risk score, the negative correlation of *CD40LG* is the most obvious (R= -0.46, p<2.2e-16) (Figure S4-S7).

Expression of ASPH and FSCN1 in different LUAD cell lines

RT-qPCR and Western blot were used to detect the relative expression of ASPH, FSCN1 in NSCLC cell lines (H1299, PC9, A549). Results Compared with normal BEAS-2B cells, all 3 NSCLC cell lines showed high FSCN1 expression, the expression of ASPH was the highest in A549 cells and lowest in H1299 cells (P< 0. 01). (Figure 7).

Effect of the expression of the immune-related genes and B cell markers on OS of LUAD patients

We finally examined the expression of *ASPH*, *FSCN1*, *MS4A1* and *CD40LG* in 60 lung adenocarcinoma tissues by immunohistochemistry. 78.33% (47/60) of LUAD patients tissue samples had positive expression of *ASPH*, 70.00% (42/60) of *FSCN1*, 21.67% (13/60) of *MS4A1*, 28.33% (17/60) of *CD40LG* (Figure 8). Based on the result of IHC of *ASPH*, *FSCN1*, *MS4A1* and *CD40LG*, the patients were divided into 2 groups (negative group and positive group); Table 4 showed the characteristics of both groups. We found that the positive expression of *ASPH*, *FSCN1*, *MS4A1* and *CD40LG* had a correlation with the TNM stage, cellular differentiation and the lymph node metastasis (p<0.05). But were not associated with the age and sex(p>0.05). Then The effect of the immune related genes on prognosis of LUAD patients was verified by Kaplan–Meier. Univariate Cox regression analysis suggested that the expression of *ASPH* (HR=0.608; 95% CI, 0.421~0.795), *FSCN1* (HR=0.684; 95% CI, 0.482~0.897), *MS4A1* (HR=0.741, 95%CI=0.624~0.891) and *CD40LG* (HR=0.653, 95%CI=0.437~0.833) were significantly associated with overall survival (OS) (Figure 9).

Table 4
Baseline characteristics of patients.

Clinical pathological characteristic	N	ASPH		P	FSCN1		P	MS4A1		P	CD40LG		P
		Positive	Negative		Positive	Negative		Positive	Negative		Positive	Negative	
Age(t/yr)							0.3561			0.4411			0.2017
≥60	38	29	9	0.3132	26	12		9	29		10	28	
<60	22	18	4		16	6		4	18		7	15	
Sex							0.5112			0.3371			0.2146
Male	33	22	11	0.4172	24	9		8	25		9	23	
Female	27	20	7		18	9		5	22		8	19	
Histological differentiation							0.0339			0.0277			0.0230
High or middle differentiation	21	13	7	0.0266	13	8		8	13		9	12	
Low or no differentiation	39	34	5		29	10		5	24		8	31	
TNM stage							0.0291			0.0433			0.0451
I-	35	27	8	0.0328	23	12		8	27		8	27	
-	25	20	5		19	6		5	20		9	16	
Lymph node metastasis							0.0346			0.0183			0.0147
No	26	19	7	0.0224	18	8		8	18		11	15	
Yes	34	28	6		24	10		5	29		6	28	

Discussion

Lung cancer is still one of the deadliest cancers worldwide, in which adenocarcinoma is the most common histological subtype. Chemotherapy, radiotherapy, targeted therapy and immunotherapy are the most common therapeutic methods for lung adenocarcinoma (36), due to its molecular complexity and cellular heterogeneity, the effect of the treatment is unsatisfactory. And the shortage of effective prognostic biomarkers to guide cancer therapy is one of the reasons for the poor prognosis. Several studies confirmed that the interaction between the tumor and its immune microenvironment is crucial in the development and progression of the tumor. The emergence of cancer cells often occurs in densely infiltrated inflammatory environments (37), and the immunoscore has been defined to quantify the in situ immune infiltrate by Galon J et al (38).

Due to the close relationship between tumor microenvironment and immunotherapy, it is necessary to find the immune-related genes related to the prognosis of LUAD patients and construct the relevant immune model, which can provide guidance for the immunotherapy of LUAD. Our study is an integrated bioinformatic analysis of publicly available datasets, underscoring the potential to reveal molecular characteristics and clinical significance by analyzing of DEIGs in LUAD. What's more, an individualized immune prognostic model based on DEIGs was developed for LUAD.The risk score calculated by this model independently predicted the outcome of patients with LUAD, and we also evaluated the infiltration of immune cells by exploring the relationship between the model and immune cells. These results indicate that the immune-related risk prediction model constructed by us is of great significance for predicting the prognosis of LUAD patients and may provide new immunotherapeutic targets.

Although the significance of DEIGs in tumor progression and immunotherapeutics has been confirmed already (39–41), the molecular mechanisms and clinical significance are unclear. We found several DEIGs significantly involved in the tumorigenesis and development of LUAD and built an immune-related ceRNA network which may perform a variety of biological functions and influence immune status in the human body and participate in the occurrence and development of various tumors (42). The indepth exploration of their molecular mechanisms was analyzed by bioinformatics. We found that the MAPK (mitogen-activated protein kinases) signaling pathway was the top enriched pathway from the 117 target genes. MAPKs are intracellular class of serine/threonine protein kinases (43), and lung adenocarcinoma has been associated with mutations that activate MAPK pathway in previous studies (44, 45). As expected, functional enrichment analysis indicated that the DEIGs were mainly involved in immune and inflammatory responses. Furthermore, a PPI network was constructed for the 117 target genes, among which, 10 hub genes were identified by cytoscape. Among these hub genes, five of them have been reported, including *FZD4*, *PDIA6*, *CDH2*, *CKAP4* and *SPP1*, a possible connection between *SH3GL2* and *CP* and LUAD has also been reported (46, 47), but mechanism is unclear. Until now, the function and mechanism of SYT1, TFRC or REPS2 in LUAD have not been reported (48–51). The network will be useful to provide information for studying its function and molecular mechanism in the future.

The 117 ceRNA network target genes were used in the modeling process. Although previous researchers have also modeling for LUAD patients' survival prediction (14, 52, 53), no study ever proposed a signature that chose the DEIGs which is also the ceRNA network target genes as the endpoint. The risk prediction model of 10 immune genes has not been studied before. The prognostic model based on ten DEIGs which was proved useful in prognostic predictions, and correlated with tumor burden, tumor stage, and metastasis. Several studies have shown that ASPH is highly expressed in the tumor tissues of patients with small-cell lung cancer, colon cancer, malignant glioma, hepatocellular carcinoma, cholangiocarcinoma and pancreatic cancer, and can affect the migration ability of tumor cells and disease progression (54). It is reported that ASPH can induce antigen-specific activation of CD4+ and CD8+T cells in human peripheral blood monocytes(55). Pinar Kanlikilicer et al. found that exosomal miRNA confers chemo-resistance via targeting CAV1/p-gp/M2-type macrophage axis in ovarian cancer(56). Recent research revealed that *FKBP4* is a member of the immunophilin protein family, which plays a role in immunoregulation and basic cellular processes involving protein folding and trafficking associated with HSP90(57, 58). Meanwhile, there is plenty of evidence that *GRIK2* and *CKAP4* has close connection with the initiation, progression and prognosis of various malignancies including lung cancer(59–61). Recent studies have confirmed that *FSCN1* is up-regulated in a variety of tumors, and can be used as a tumor marker in Hodgkin's lymphoma and Epstein Barr virus-associated lymphoma (62), as a predictor of prognosis and recurrence time of pancreatic ductal adenocarcinoma, and can promote immune escape of tumor cells(63, 64). These results corroberated the prognostic value of our model. The remaining genes merit further study to explore their potential as prognostic biomarkers for LUAD patients.

Furthermore, the DEIGs could serve not only as a prognostic indicator, but also as an immune status indicator. Lots of studies demonstrated that the tumor-infiltrating immune cells play an important role in regulating tumor growth, metastasis and angiogenesis of lung cancer. TIL-Bs plays a bidirectional regulating role. Wang SS et al. showed that high-density TIL-Bs was closely related to the good prognosis of lung cancer patients (65). Kinoshita T et al. showed that high expression levels of TIL-Bs, CD4+T cells and CD8+T cells in the tumor microenvironment of NSCLC patients predicted long disease-free survival (66).These reports are in line with our results. We explored the relationships between the risk score of our model and immune cell infiltration to investigate the tumor–immune interactions. Our analysis indicated that the risk score of our model was inversely related to the infiltration of B cell, CD4+ T cell and dendritic cell. The high-risk patients had lower infiltration levels of B cell, CD4+ T cell and dendritic cell. Thus, our model predicted risk score could serve as an indicator for immune infiltration status. We have also validated the expression of *ASPH*, *FSCN1*, *MS4A1* and *CD40LG* in lung cancer cells and tissues, and revealed that the expression of *ASPH*, *FSCN1*, *MS4A1* and *CD40LG* are independent prognostic factors. Furthermore, high levels of *ASPH* and *FSCN1* and low levels of *MS4A1* and *CD40LG* expression are associated with poor overall survival in lung adenocarcinoma. These results suggest that our model can be used as a reliable risk-prediction tools in patients with LUAD.

In conclusion, in this study, we successfully constructed a risk prediction model of 10 immune genes, and systematically analyzed their prognostic value in LUAD. The model constructed in this study is an independent prognostic factor for survival in patients with LUAD. Our preliminary results give us a possible hint to discuss the relationship between immune related genes and the prognosis of LUAD. Through further biological function analysis, we can understand the function of these DEIGs in the occurrence and development of LUAD, thus providing a new idea for the treatment of LUAD. However, there were also some limitations of our studies, rendering further studies into the mechanisms of DEIGs modulated LUAD progression necessary.

Declarations

Availability of data and materials

All data generated or analyzed during this study are included in this published article and its Supplementary Information files. The datasets generated and/or analyzed during the current study are available in the TCGA repository(https://portal.gdc.cancer.gov/). The immune-related genes were derived from InnateDB (https://www.innatedb.com/). While the estimated infiltration abundance of immune cells of LUAD samples were obtained by TIMER (https://cistrome.shinyapps.io/timer/).

Acknowledgements

This work was supported by National Natural Science Foundation of Shaanxi (No. 2019JQ-566) and Incubation Project of National Natural Science Foundation of Tumor Hospital of Shaanxi Province (No. SC211004).

Contributions

Yang Zhai and Qian Chen contributed to the conception of the study. Lina Li and Jingjin Li, contributed significantly to analysis and manuscript preparation; Xu Li and Rui Xu performed the data analyses and wrote the manuscript; Bin Liu has made contribution to the supplementary experiments and manuscript modification; Yili Zhang and Yuzhen Wang helped perform the analysis with constructive discussions. All authors reviewed the manuscript.We thank Miaomiao Jiang and Xiaoyun Huang from Zhiyu Center for Systems Biology (Intelliphecy Inc.) for support with Bioinformatics.

Ethics approval and consent to participate

The studies involving human participants were reviewed and approved by Ethics Committee of Tumor Hospital of Shaanxi Province. Written informed consent for participation was not required for this study in accordance with the national legislation and the institutional requirements.

Consent for publication

No consent is required in this study.

Competing interests

These authors declare no conflicts of interest.

References

1. Global Burden of Disease Cancer, C. *et al.* Global, Regional, and National Cancer Incidence, Mortality, Years of Life Lost, Years Lived With Disability, and Disability-Adjusted Life-Years for 29 Cancer Groups, 1990 to 2017: A Systematic Analysis for the Global Burden of Disease Study. *JAMA Oncol* 5, 1749–1768, doi:10.1001/jamaoncol.2019.2996 (2019).
2. Vossler, J. D., Abdul-Ghani, A., Tsai, P. I. & Morris, P. T. Outcomes of Anatomic Lung Resection for Cancer are Better When Performed by Cardiothoracic Surgeons. *Ann Thorac Surg*, doi:10.1016/j.athoracsur.2020.06.022 (2020).
3. Kneuertz, P. J. *et al.* Prognostic value and therapeutic implications of expanded molecular testing for resected early stage lung adenocarcinoma. *Lung Cancer* 143, 60–66, doi:10.1016/j.lungcan.2020.03.012 (2020).
4. Tammela, T. *et al.* A Wnt-producing niche drives proliferative potential and progression in lung adenocarcinoma. *Nature* 545, 355–359, doi:10.1038/nature22334 (2017).
5. Jang, H. J. *et al.* Transcriptome-based molecular subtyping of non-small cell lung cancer may predict response to immune checkpoint inhibitors. *J Thorac Cardiovasc Surg* 159, 1598-1610 e1593, doi:10.1016/j.jtcvs.2019.10.123 (2020).
6. Zhang, Z. *et al.* Immune checkpoint inhibitors for treatment of advanced gastric or gastroesophageal junction cancer: Current evidence and future perspectives. *Chin J Cancer Res* 32, 287–302, doi:10.21147/j.issn.1000-9604.2020.03.02 (2020).
7. Gao, J. *et al.* Neoadjuvant PD-L1 plus CTLA-4 blockade in patients with cisplatin-ineligible operable high-risk urothelial carcinoma. *Nat Med*, doi:10.1038/s41591-020-1086-y (2020).
8. Cummings, A. L., Santoso, K. M. & Goldman, J. W. KEYNOTE-021 cohorts D and H suggest modest benefit in combining ipilimumab with pembrolizumab in second-line or later advanced non-small cell lung cancer treatment. *Transl Lung Cancer Res* 8, 706–709, doi:10.21037/tlcr.2019.08.11 (2019).
9. Reck, M. *et al.* Updated Analysis of KEYNOTE-024: Pembrolizumab Versus Platinum-Based Chemotherapy for Advanced Non-Small-Cell Lung Cancer With PD-L1 Tumor Proportion Score of 50% or Greater. *J Clin Oncol* 37, 537–546, doi:10.1200/JCO.18.00149 (2019).
10. Wu, Y. L. *et al.* Nivolumab Versus Docetaxel in a Predominantly Chinese Patient Population With Previously Treated Advanced NSCLC: CheckMate 078 Randomized Phase III Clinical Trial. *J Thorac Oncol* 14, 867–875, doi:10.1016/j.jtho.2019.01.006 (2019).
11. DeBerardinis, R. J. Tumor Microenvironment, Metabolism, and Immunotherapy. *N Engl J Med* 382, 869–871, doi:10.1056/NEJMcibr1914890 (2020).
12. Boys, J. & Onaitis, M. Commentary: Breaking down non-small cell lung cancer tumor microenvironment heterogeneity and predicting response to immune checkpoint inhibitors. *J Thorac Cardiovasc Surg* 159, 1612–1613, doi:10.1016/j.jtcvs.2019.11.097 (2020).
13. Li, B., Cui, Y., Diehn, M. & Li, R. Development and Validation of an Individualized Immune Prognostic Signature in Early-Stage Nonsquamous Non-Small Cell Lung Cancer. *JAMA Oncol* 3, 1529–1537, doi:10.1001/jamaoncol.2017.1609 (2017).
14. Li, J., Li, X., Zhang, C., Zhang, C. & Wang, H. A signature of tumor immune microenvironment genes associated with the prognosis of nonsmall cell lung cancer. *Oncol Rep* 43, 795–806, doi:10.3892/or.2020.7464 (2020).
15. Colaprico, A. *et al.* TCGAbiolinks: an R/Bioconductor package for integrative analysis of TCGA data. *Nucleic Acids Res* 44, e71, doi:10.1093/nar/gkv1507 (2016).
16. Frankish, A. *et al.* GENCODE reference annotation for the human and mouse genomes. *Nucleic Acids Res* 47, D766-D773, doi:10.1093/nar/gky955 (2019).
17. Breuer, K. *et al.* InnateDB: systems biology of innate immunity and beyond--recent updates and continuing curation. *Nucleic Acids Res* 41, D1228-1233, doi:10.1093/nar/gks1147 (2013).
18. Li, T. *et al.* TIMER: A Web Server for Comprehensive Analysis of Tumor-Infiltrating Immune Cells. *Cancer Res* 77, e108-e110, doi:10.1158/0008-5472.CAN-17-0307 (2017).
19. Love, M. I., Huber, W. & Anders, S. Moderated estimation of fold change and dispersion for RNA-seq data with DESeq2. *Genome Biol* 15, 550, doi:10.1186/s13059-014-0550-8 (2014).
20. Robinson, M. D., McCarthy, D. J. & Smyth, G. K. edgeR: a Bioconductor package for differential expression analysis of digital gene expression data. *Bioinformatics* 26, 139–140, doi:10.1093/bioinformatics/btp616 (2010).
21. Yu, G., Wang, L. G., Han, Y. & He, Q. Y. clusterProfiler: an R package for comparing biological themes among gene clusters. *OMICS* 16, 284–287, doi:10.1089/omi.2011.0118 (2012).
22. Li, J. H., Liu, S., Zhou, H., Qu, L. H. & Yang, J. H. starBase v2.0: decoding miRNA-ceRNA, miRNA-ncRNA and protein-RNA interaction networks from large-scale CLIP-Seq data. *Nucleic Acids Res* 42, D92-97, doi:10.1093/nar/gkt1248 (2014).
23. Kanehisa, M., Furumichi, M., Sato, Y., Ishiguro-Watanabe, M. & Tanabe, M. KEGG: integrating viruses and cellular organisms. Nucleic Acids Res 49, D545-D551, doi:10.1093/nar/gkaa970 (2021).
24. Shannon, P. *et al.* Cytoscape: a software environment for integrated models of biomolecular interaction networks. *Genome Res* 13, 2498–2504, doi:10.1101/gr.1239303 (2003).

25. Szklarczyk, D. *et al.* STRING v11: protein-protein association networks with increased coverage, supporting functional discovery in genome-wide experimental datasets. *Nucleic Acids Res* 47, D607-D613, doi:10.1093/nar/gky1131 (2019).
26. Friedman, J., Hastie, T. & Tibshirani, R. Regularization Paths for Generalized Linear Models via Coordinate Descent. *J Stat Softw* 33, 1–22 (2010).
27. Dorandish, S. *et al.* Regulation of amyloid-beta levels by matrix metalloproteinase-2/9 (MMP2/9) in the media of lung cancer cells. *Sci Rep* **11**, 9708, doi:10.1038/s41598-021-88574-0 (2021).
28. Sun, J., Xin, K., Leng, C. & Ge, J. Down-regulation of SNHG16 alleviates the acute lung injury in sepsis rats through miR-128-3p/HMGB3 axis. *BMC Pulm Med* **21**, 191, doi:10.1186/s12890-021-01552-0 (2021).
29. Liu, M. *et al.* Cytoplasmic liver kinase B1 promotes the growth of human lung adenocarcinoma by enhancing autophagy. *Cancer Sci* **109**, 3055–3067, doi:10.1111/cas.13746 (2018).
30. Wang, H. *et al.* Circular RNA MAT2B promotes migration, invasion and epithelial-mesenchymal transition of non-small cell lung cancer cells by sponging miR-431. *Cell Cycle*, 1–11, doi:10.1080/15384101.2021.1956106 (2021).
31. Ge, X. *et al.* EGFR tyrosine kinase inhibitor Almonertinib induces apoptosis and autophagy mediated by reactive oxygen species in non-small cell lung cancer cells. *Hum Exp Toxicol*, 9603271211030554, doi:10.1177/09603271211030554 (2021).
32. Zhang, Z. *et al.* Antitumor Effects of 3-bromoascochlorin on Small Cell Lung Cancer via Inhibiting MAPK Pathway. *Cell Biol Int*, doi:10.1002/cbin.11674 (2021).
33. Fang, C. *et al.* A innovative prognostic symbol based on neutrophil extracellular traps (NETs)-related lncRNA signature in non-small-cell lung cancer. *Aging (Albany NY)* **13**, 17864–17879, doi:10.18632/aging.203289 (2021).
34. Fung, A. S. & Leighl, N. B. Advancing the systemic therapy of. lung cancer: quality or quantity? Lancet Oncol 21, 322–324, doi:10.1016/S1470-2045(20)30076-0 (2020).
35. Sethi, R. S., Brar, R. S., Singh, O. & Singh, B. Immunolocalization of pulmonary intravascular macrophages, TLR4, TLR9 and IL-8 in normal and Pasteurella multocida-infected lungs of water buffalo (Bubalus bubalis). *J Comp Pathol* 144, 135–144, doi:10.1016/j.jcpa.2010.08.003 (2011).
36. Hewitt, S. M., Baskin, D. G., Frevert, C. W., Stahl, W. L. & Rosa-Molinar, E. Controls for immunohistochemistry: the Histochemical Society's standards of practice for validation of immunohistochemical assays. *J Histochem Cytochem* 62, 693–697, doi:10.1369/0022155414545224 (2014).
37. Hanahan, D. & Weinberg, R. A. Hallmarks of cancer: the next generation. *Cell* 144, 646–674, doi:10.1016/j.cell.2011.02.013 (2011).
38. Galon, J. *et al.* Towards the introduction of the 'Immunoscore' in the classification of malignant tumours. *J Pathol* 232, 199–209, doi:10.1002/path.4287 (2014).
39. Chen, H. *et al.* The immune response-related mutational signatures and driver genes in non-small-cell lung cancer. *Cancer Sci* 110, 2348–2356, doi:10.1111/cas.14113 (2019).
40. Wei, X. *et al.* Effects of ALOX5, IL6R and SFTPD gene polymorphisms on the risk of lung cancer: A case-control study in China. *Int Immunopharmacol* 79, 106155, doi:10.1016/j.intimp.2019.106155 (2020).
41. Dimitrakopoulos, F. D. *et al.* Expression of Immune System-Related Membrane Receptors CD40, RANK, BAFFR and LTbetaR is Associated with Clinical Outcome of Operated Non-Small-Cell Lung Cancer Patients. *J Clin Med* 8, doi:10.3390/jcm8050741 (2019).
42. Wang, X. *et al.* The construction and analysis of the aberrant lncRNA-miRNA-mRNA network in non-small cell lung cancer. *J Thorac Dis* 11, 1772–1778, doi:10.21037/jtd.2019.05.69 (2019).
43. Zhang, Y. X., Yuan, J., Gao, Z. M. & Zhang, Z. G. LncRNA TUC338 promotes invasion of lung cancer by activating MAPK pathway. *Eur Rev Med Pharmacol Sci* 22, 443–449, doi:10.26355/eurrev_201801_14193 (2018).
44. Dong, Z. Y., Zhou, Y. R. & Wang, L. X. HDAC1 is indirectly involved in the epigenetic regulation of p38 MAPK that drive the lung cancer progression. *Eur Rev Med Pharmacol Sci* 22, 5980–5986, doi:10.26355/eurrev_201809_15932 (2018).
45. Fang, Y. *et al.* Inactivation of p38 MAPK contributes to stem cell-like properties of non-small cell lung cancer. *Oncotarget* 8, 26702–26717, doi:10.18632/oncotarget.15804 (2017).
46. Haghjoo, N., Moeini, A. & Masoudi-Nejad, A. Introducing a panel for early detection of lung adenocarcinoma by using data integration of genomics, epigenomics, transcriptomics and proteomics. *Exp Mol Pathol* 112, 104360, doi:10.1016/j.yexmp.2019.104360 (2020).
47. Wan, X. *et al.* First-line atezolizumab in addition to bevacizumab plus chemotherapy for metastatic, nonsquamous non-small cell lung cancer: A United States-based cost-effectiveness analysis. *Cancer* 125, 3526–3534, doi:10.1002/cncr.32368 (2019).
48. Lu, H., Hao, L., Yang, H., Chen, J. & Liu, J. miRNA-34a suppresses colon carcinoma proliferation and induces cell apoptosis by targeting SYT1. *Int J Clin Exp Pathol* 12, 2887–2897 (2019).
49. Muhammad, J. S., Bajbouj, K., Shafarin, J. & Hamad, M. Estrogen-induced epigenetic silencing of FTH1 and TFRC genes reduces liver cancer cell growth and survival. *Epigenetics*, 1–17, doi:10.1080/15592294.2020.1770917 (2020).
50. Huang, Y. *et al.* TFRC promotes epithelial ovarian cancer cell proliferation and metastasis via up-regulation of AXIN2 expression. *Am J Cancer Res* 10, 131–147 (2020).
51. Zhou, Y. W. *et al.* miR-675-5p enhances tumorigenesis and metastasis of esophageal squamous cell carcinoma by targeting REPS2. *Oncotarget* 7, 30730–30747, doi:10.18632/oncotarget.8950 (2016).
52. Li, R. *et al.* Increased expression of the RNA-binding motif protein 47 predicts poor prognosis in non-small-cell lung cancer. *Oncol Lett* 19, 3111–3122, doi:10.3892/ol.2020.11417 (2020).

53. Qu, Y. *et al.* Prognostic value of immune-related genes in the tumor microenvironment of lung adenocarcinoma and lung squamous cell carcinoma. *Aging (Albany NY)* 12, 4757–4777, doi:10.18632/aging.102871 (2020).
54. Lin, Q. *et al.* ASPH-notch Axis guided Exosomal delivery of Prometastatic Secretome renders breast Cancer multi-organ metastasis. *Mol Cancer* 18, 156, doi:10.1186/s12943-019-1077-0 (2019).
55. Benelli, R. *et al.* Aspartate-beta-Hydroxylase: A Promising Target to Limit the Local Invasiveness of Colorectal Cancer. *Cancers (Basel)* 12, doi:10.3390/cancers12040971 (2020).
56. Kanlikilicer, P. *et al.* Corrigendum to 'Exosomal miRNA confers chemo resistance via targeting Cav1/p-gp/M2-type macrophage axis in ovarian cancer' [EBioMedicine 38 (2018) 100-112]. *EBioMedicine* 52, 102630, doi:10.1016/j.ebiom.2020.102630 (2020).
57. Xiong, H. *et al.* FKBP4 is a malignant indicator in luminal A subtype of breast cancer. *J Cancer* 11, 1727–1736, doi:10.7150/jca.40982 (2020).
58. Inoue, R. *et al.* GRIK2 has a role in the maintenance of urothelial carcinoma stem-like cells, and its expression is associated with poorer prognosis. *Oncotarget* 8, 28826–28839, doi:10.18632/oncotarget.16259 (2017).
59. Xiao, W. *et al.* SOX2 Promotes Brain Metastasis of Breast Cancer by Upregulating the Expression of FSCN1 and HBEGF. *Mol Ther Oncolytics* 17, 118–129, doi:10.1016/j.omto.2020.03.001 (2020).
60. Li, X., Han, X., Wei, P., Yang, J. & Sun, J. Knockdown of lncRNA CCAT1 enhances sensitivity of paclitaxel in prostate cancer via regulating miR-24-3p and FSCN1. *Cancer Biol Ther* 21, 452–462, doi:10.1080/15384047.2020.1727700 (2020).
61. Ou, C. *et al.* Targeting YAP1/LINC00152/FSCN1 Signaling Axis Prevents the Progression of Colorectal Cancer. *Adv Sci (Weinh)* 7, 1901380, doi:10.1002/advs.201901380 (2020).
62. Zhang, Y. & Lin, Q. MicroRNA-145 inhibits migration and invasion by down-regulating FSCN1 in lung cancer. *Int J Clin Exp Med* 8, 8794–8802 (2015).
63. Kimura, H. *et al.* CKAP4, a DKK1 Receptor, Is a Biomarker in Exosomes Derived from Pancreatic Cancer and a Molecular Target for Therapy. *Clin Cancer Res* 25, 1936–1947, doi:10.1158/1078-0432.CCR-18-2124 (2019).
64. Lu, G. F. *et al.* MicroRNA-671-3p promotes proliferation and migration of glioma cells via targeting CKAP4. *Onco Targets Ther* 11, 6217–6226, doi:10.2147/OTT.S177325 (2018).
65. Wang, S. S. *et al.* Tumor-infiltrating B cells: their role and application in anti-tumor immunity in lung cancer. *Cell Mol Immunol* 16, 6–18, doi:10.1038/s41423-018-0027-x (2019).
66. Kinoshita, T. *et al.* Prognostic value of tumor-infiltrating lymphocytes differs depending on histological type and smoking habit in completely resected non-small-cell lung cancer. *Ann Oncol* 27, 2117–2123, doi:10.1093/annonc/mdw319 (2016).

Figures

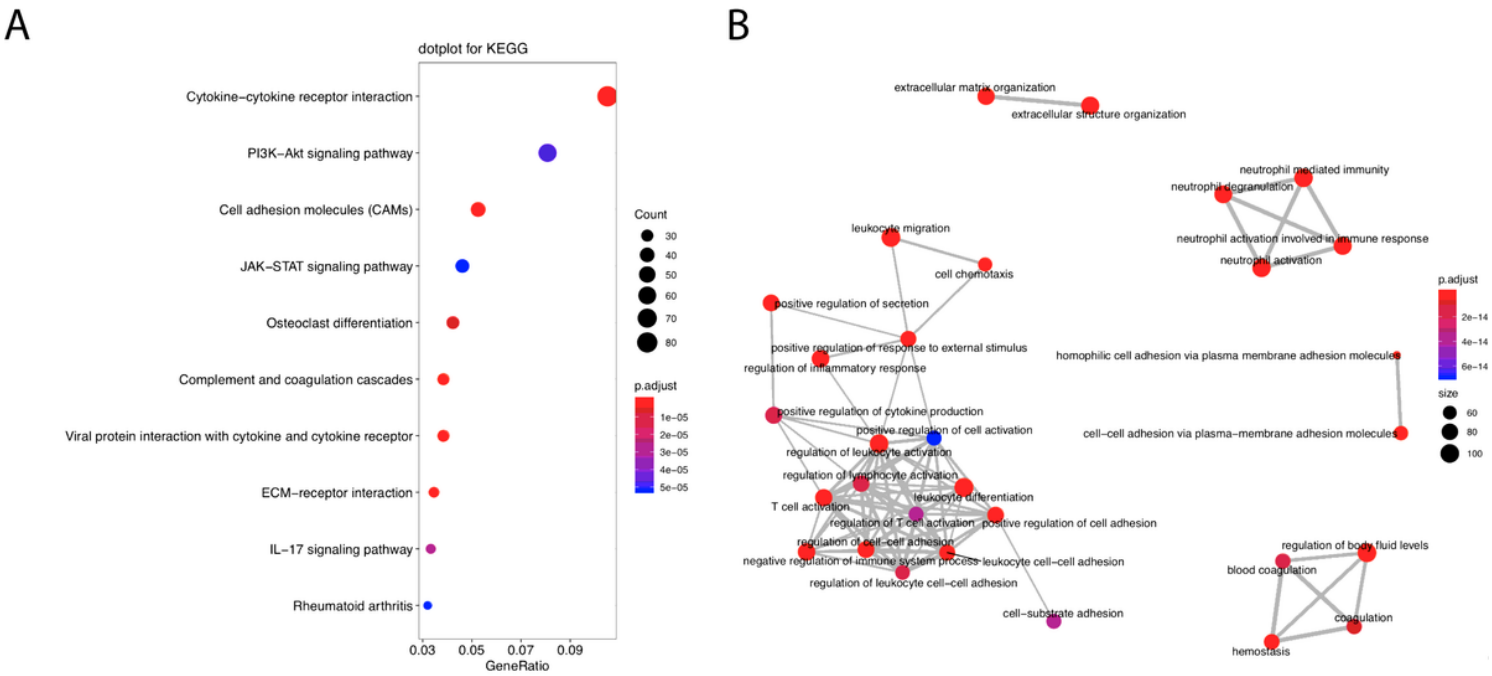

Figure 1

Gene functional enrichment of differentially expressed immune-related genes (A: Top10 enriched KEGG gene sets; B: Enrichment map organized the top30 enriched GO terms into a network with edges connecting overlapping gene sets.)

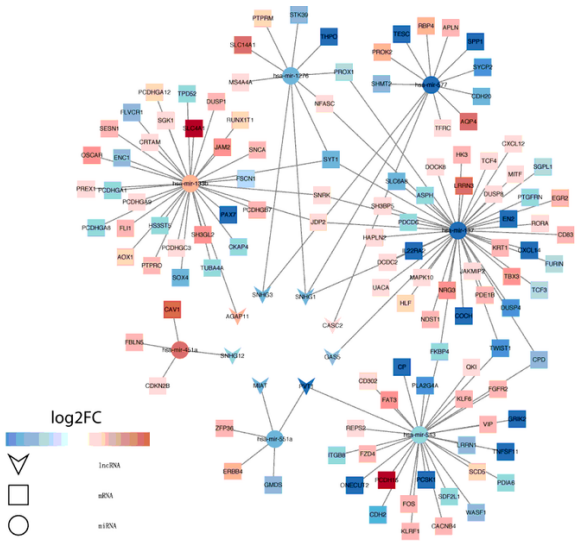

Figure 2

ceRNA network construction

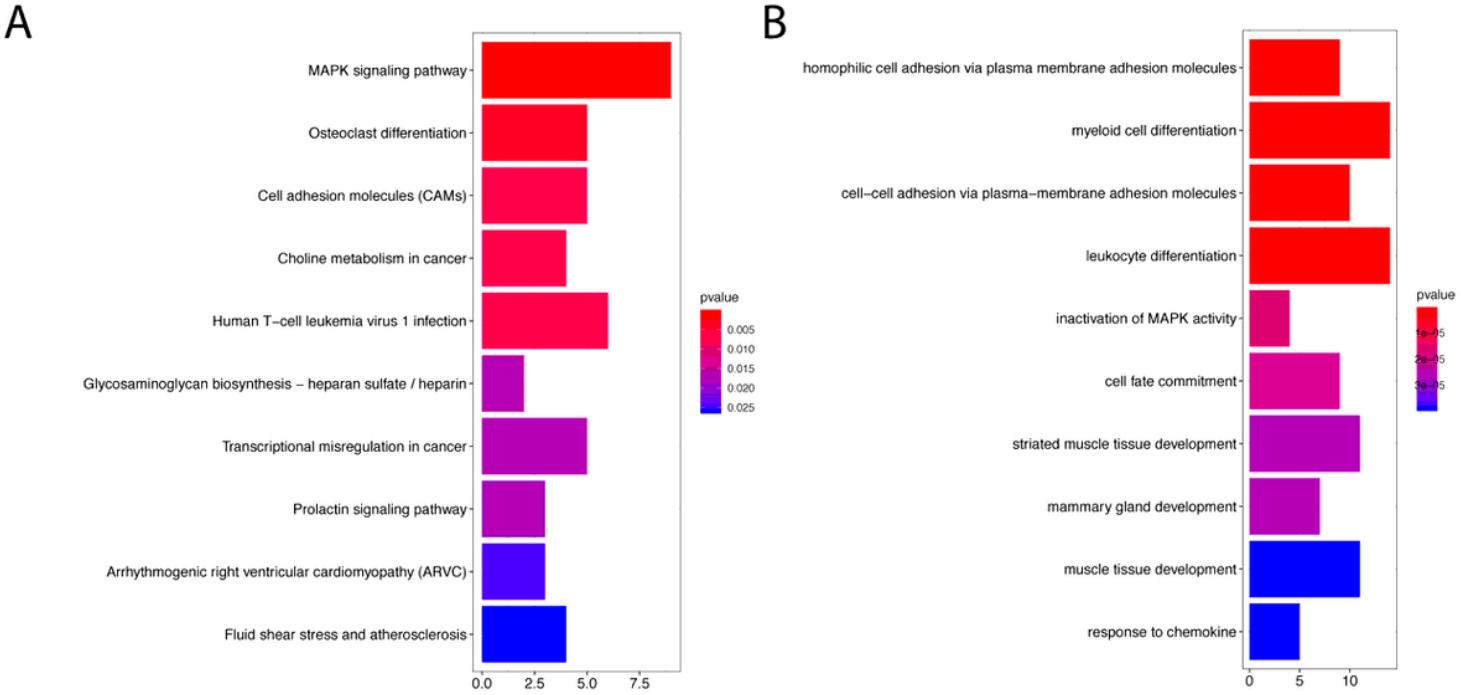

Figure 3

Gene functional enrichment of 117 target genes (A: Top10 enriched KEGG gene sets;B: Top10 enriched GO terms)

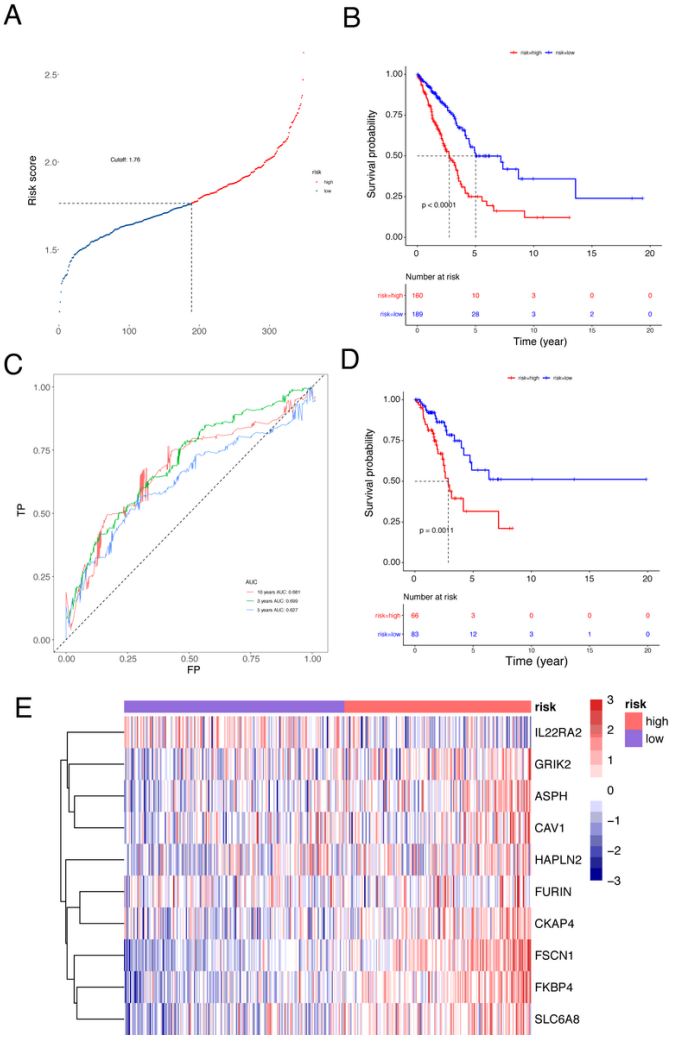

Figure 4

Identification of an immune signature predicting prognosis risk of patients in LUAD：A: determine a cutoff of risk factor and dividing samples to two group accordingly; B: survival analysis of the training dataset; C: ROC curve validation of prognostic value of the prognostic index; D: survival analysis in the testing data; E: Statistical analysis was performed by R (3.6.1). Heatmaps were generated using R package pheatmap (1.0.12) which distinct gene expression profiles of the cases belonging to the high and low risk score groups：

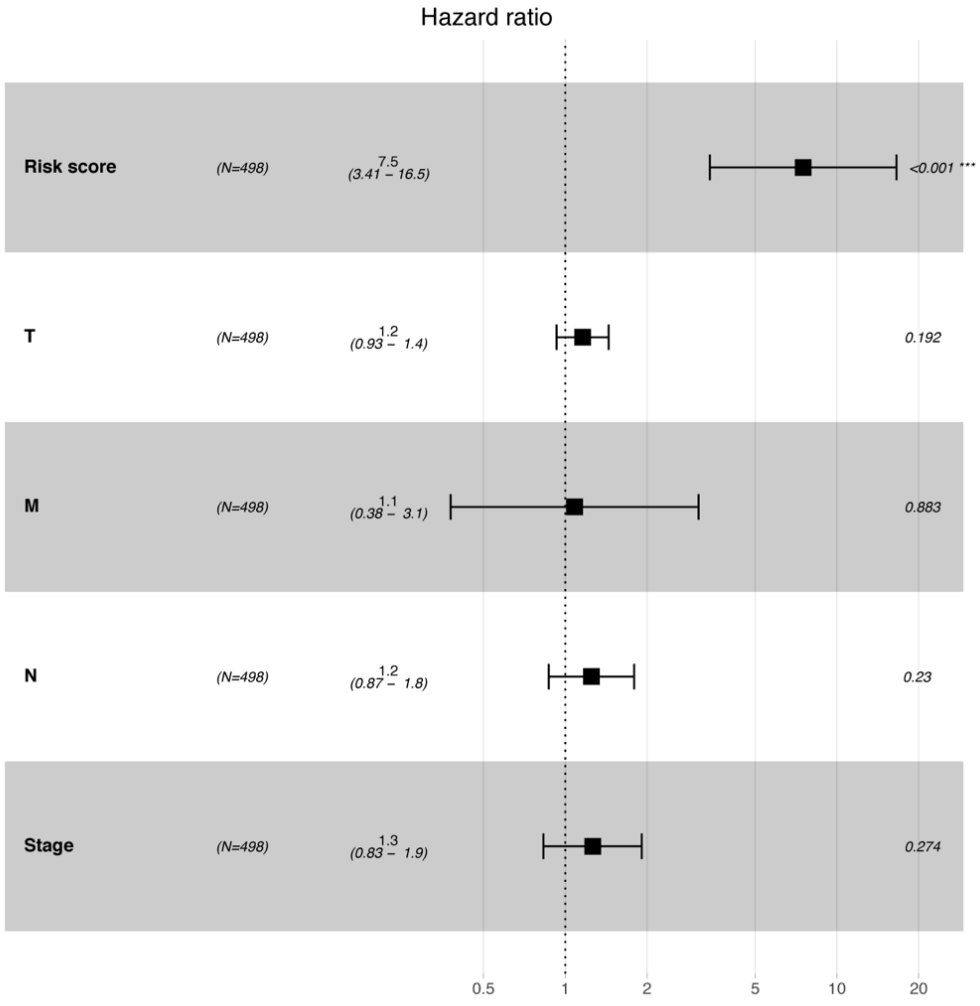

Figure 5

Multivariate cox regression analysis

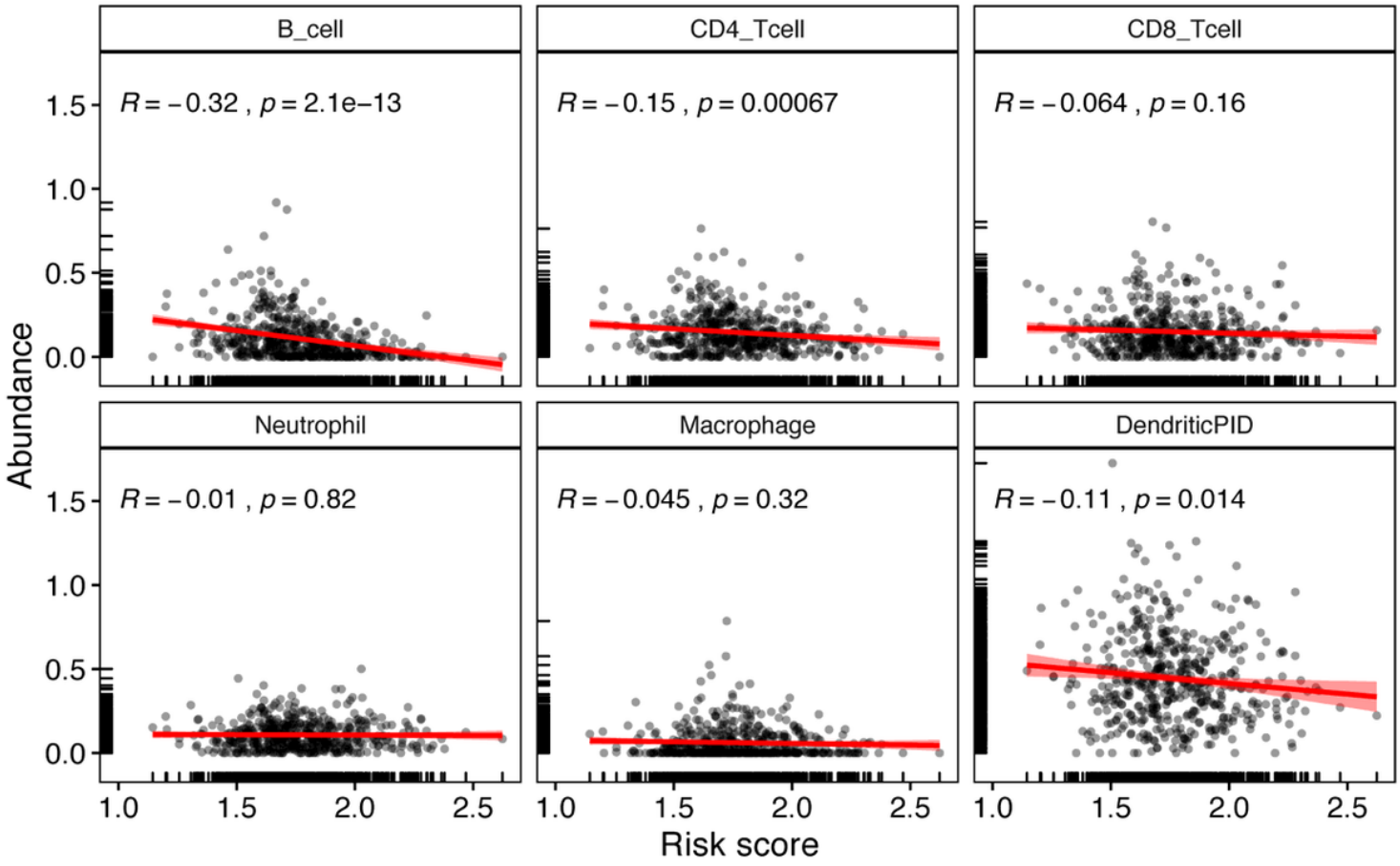

Figure 6

Relationships between the risk score and estimated infiltration abundances of immune cells.

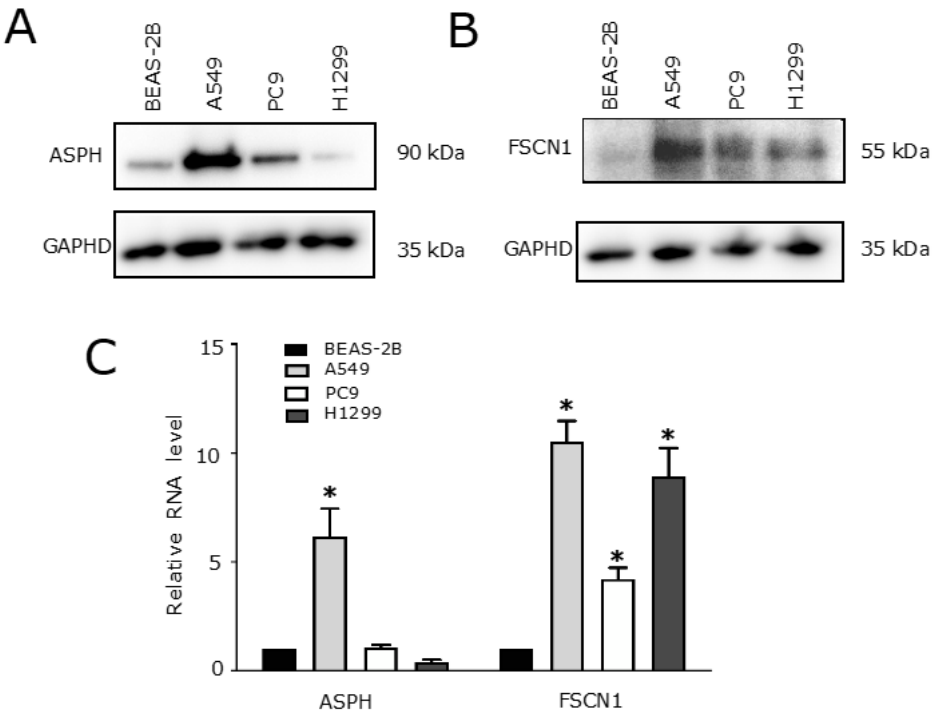

Figure 7

The expression of ASPH and FSCN1 in human NSCLC cell lines. (A) The expression of ASPH detected by Western blot in different cell lines; (B) The expression of FSCN1 detected by Western blot in different cell lines; The 'full-length blots/gels are presented in Supplementary Figure S9.(C) RT-qPCR analysis for ASPH and FSCN1 mRNA expression in different cell lines. The data are presented as mean ± SD of 3 independent experiments. The bar graph shows the relative expression in each cell line. (*P < 0.01 compared with the control cells).

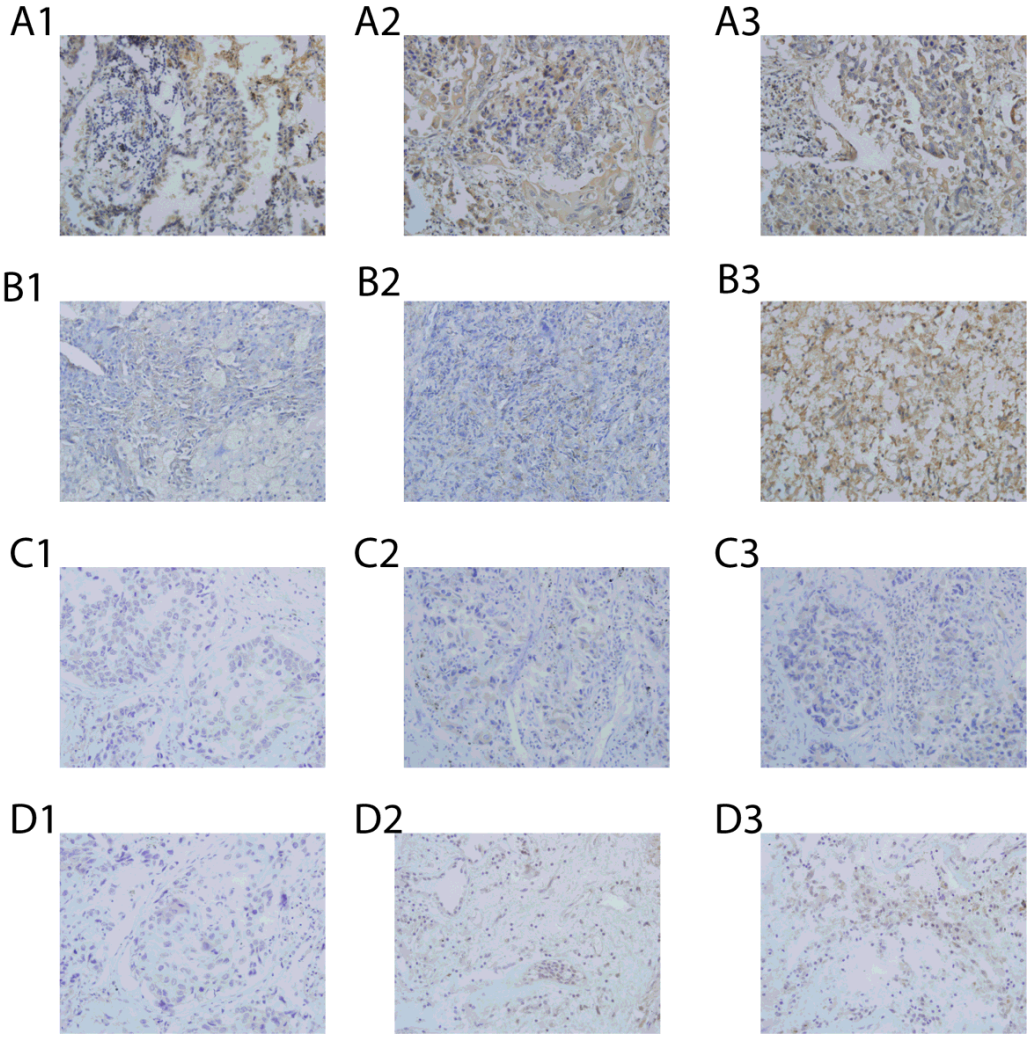

Figure 8

Immunohistochemical staining of ASPH, FSCN1, MS4A1 and CD40LG protein in LUAD tissues (magnification, x200). (Immunohistochemical expression of ASPH in LUAD tissues (A1-A3), FSCN1 (B1-B3) , MS4A1(C1-C3) and CD40LG (D1-D3). (A1,B1,C1,D1) weak expression, (A2,B2,C2,D2) moderate expression and (A3,B3,C3,D3) strong expression.)

Figure 9

The correlation between ASPH, FSCN1, MS4A1, CD40LG and OS of LUAD patients. (A: Median survival time (MS) of LUAD patients with ASPH (-) and ASPH (+) was 40.00 months (95% CI, 32.13 to 45.61) and 22.00 (95% CI,15.20 to 28.80), respectively, P=0.006. B: The MS of patients with FSCN1 (-) and FSCN1 (+) was 32.00 months (95% CI,27.33 to 36.15) and 22.50 (95% CI, 18.12 to 26.47), respectively, P=0.0107. C: The MS of patients with MS4A1 (-) and MS4A1 (+) was 23.00 months (95% CI,18.14 to 27.92) and 40.00 (95% CI, 35.12 to 46.03), respectively, P=0.0104. D: The MS of patients with CD40LG (-) and CD40LG (+) was 23.00 months (95% CI,16.54 to 27.12) and 31.00 (95% CI, 23.91 to 35.43), respectively, P=0.004.)

Supplementary Files

This is a list of supplementary files associated with this preprint. Click to download.

- supplement.pdf